

RSC Advances



This is an *Accepted Manuscript*, which has been through the Royal Society of Chemistry peer review process and has been accepted for publication.

Accepted Manuscripts are published online shortly after acceptance, before technical editing, formatting and proof reading. Using this free service, authors can make their results available to the community, in citable form, before we publish the edited article. This *Accepted Manuscript* will be replaced by the edited, formatted and paginated article as soon as this is available.

You can find more information about *Accepted Manuscripts* in the [Information for Authors](#).

Please note that technical editing may introduce minor changes to the text and/or graphics, which may alter content. The journal's standard [Terms & Conditions](#) and the [Ethical guidelines](#) still apply. In no event shall the Royal Society of Chemistry be held responsible for any errors or omissions in this *Accepted Manuscript* or any consequences arising from the use of any information it contains.

The *in-situ* formation of platinum nanoparticles and its catalytic role in electroactive phase formation in poly(vinylidene fluoride): A simple preparation of multifunctional poly(vinylidene fluoride) films doped with platinum nanoparticles

Sujoy Kumar Ghosh, Md. Meheeb Alam, Dipankar Mandal*

Organic Nano-Piezoelectric Device Laboratory

Department of Physics, Jadavpur University, Kolkata-700032, India

ABSTRACT: A simple route of *in-situ* platinum nanoparticles (Pt-NPs) synthesis is prescribed. A trace amount (0.048 mM) of platinum precursor promotes the electroactive phase transformations ($\alpha \rightarrow \beta$ and γ -phase) in poly(vinylidene fluoride) (PVDF) implying a new catalytic role of Pt-NPs. Furthermore, a complete conversion (~99 %) to electroactive phase is achieved by simply controlling the platinum precursor amount. The PVDF film doped with Pt-NPs exhibits various functionalities, *i.e.*, human touch response, enhanced ferroelectric remnant polarization and intense photoluminance in UV-region. Apart from conventional piezoelectric sensors and actuators, it naturally lends to futuristic applications as vibration based energy harvester, ferroelectric non-volatile memory element and large area coverage lightweight foldable optoelectronic device.

Keywords: Platinum Nanoparticles (Pt-NPs), Electroactive Phase, PVDF, Piezoelectric Energy Harvester, UV-emitter, Multifunction Flexible Film, Tactile Sensor.

INTRODUCTION

The advanced polymers as multifunctional materials in robust real-world applications have received tremendous attention over the last decades. Among them poly(vinylidene fluoride) (PVDF) is the best suitable choices due to its distinct applications in diverse field, *e.g.*, energy scavenging, storage, sensors, actuators and many others.¹ PVDF (chemical formula: $(\text{CH}_2\text{CF}_2)_n$), a semi-crystalline material exhibits at least four different crystalline polymorphs referred to as α ($TGT\bar{G}$), β ($TTTT$), γ ($T_3GT_3\bar{G}$) and δ (polarized α , *i.e.*, α_p -phase)-phases, depending on their macromolecular chain conformations of *trans* (*T*) and *gauche* (*G*) linkages.² In order to use PVDF in sensor and actuators fabrication, electroactive crystalline phases, namely β and γ -phases are preferred due to their piezo-, ferro- and pyro-electric properties.²⁻⁵ Among them β -phase has special attention due to high piezoelectric coefficient.² On the other hand due to non-early saturation of the electrical polarization and higher energy density, γ -phase is also suitable for energy storage device.⁶ As a consequence, so far tremendous efforts have been paid to induce the electroactive β and γ -phases, such as mechanical stretching, application of high pressure, heat control spin coating, addition of hydrated metal salts, formation of a nanocomposite, blending with PMMA, polarization via an applied electric field, electrospinning and many others.⁵ However, to fabricate mechanically flexible yet robust smart sensors (electrical or/and optical) and actuators, much importance is laid on paying attention to the way the NPs are incorporated into the PVDF matrix as the morphology and density of the NPs affect the overall functionality.⁷ In this context, *in-situ* preparation of metal NPs and its doping in PVDF have continually proven to be the elite materials in multifunctional approach towards sensor technology, it also includes the very interesting redox properties of Pt-NPs.⁸⁻¹¹

Herein, we report an *in-situ* preparation of platinum nanoparticles (Pt-NPs) and its successful doping in PVDF by a simple, single step and scalable procedure. Pt-NPs act here as a new type of catalyst for crystallographic phase transformation in PVDF, *viz.*, $\alpha \rightarrow \beta$ and γ -phase. In order to represent the multifunctionality of Pt-NPs doped PVDF films, we have demonstrated the piezo-sensitivity, ferroelectric response, and photoemission properties. It indicates a futuristic material for fabricating the flexible tactile sensor and also an energy harvester that may have the self powering capability to tiny electric devices. Additionally, *in-situ* Pt-NPs impregnated PVDF films give rise an intense UV-photoluminescence (PL), establishing as promising material for next generation optoelectronic devices, such as, Photo sensors, UV-laser emitters, solar cell, light emitting diodes and so forth.¹² It is well accepted that room-temperature PL spectra of ZnO nanostructures typically consist of intense UV emission. However, limitation of application arises as these materials consist of few visible bands due to defects and/or impurities.¹² Though, many successful attempts have already been reported to obtain the isolated PL in UV-region using several typical nano-structures, made with defect free 3D ZnO rod,¹³ CdS-Pt nanorod heterostructures,¹⁴ Mg doped SnO₂ nano-crystals,¹⁵ Pt-NPs capped ZnMgO films¹⁶ and so on. However, the preparation of these materials dealt with expensive and multistep processes. In this context, our attempt to prepare the UV-emitting Pt-NPs doped PVDF films is simple and cost-effective. It should be noted that recently, Kang et al. reported a weak micro-photoluminescence (PL) in visible region from Pt nano-island films.¹⁷ However, UV-photoemission has not yet been reported from Pt-nanostructures. In contrast, first time we have observed an intense photoemission in UV-region from flexible Pt-NPs doped PVDF films, relevant for futuristic photonic smart sensor fabrication.

In addition, the use of large amount of filler content,¹⁸ traditional stretching technique¹⁹ and few more expensive methodology *i.e.* swift heavy ion irradiation,²⁰ electron irradiation²¹ etc. can be avoided in sensor fabrication as these processes deteriorate the PVDF film quality (*i.e.* flexibility, homogeneity, electrical breakdown strength, fatal polarization etc.). In this context, the intense, broad UV-photoemission and legion functionality from Pt-NPs doped flexible PVDF films may aid the significant importance along with enhanced electroactive properties. It should also be noted that as PVDF membrane is being utilizing as proton exchange membrane (PEM) fuel cell,²² therefore it can be anticipated that Pt-NPs embedded PVDF membranes might have tremendous proton exchange functionality in PEM based fuel cells due to excellent adsorption and dissociation of hydrogen, oxygen, and other molecules by Pt-NPs.

EXPERIMENTAL

Methodology. PVDF solutions were prepared by dissolving PVDF (Sigma-Aldrich, USA, $M_w = 275\ 000$) in N, N-dimethyl formamide (DMF, Merck, India) without and with addition of several (Supporting Information, Methodology Sec.) wt% (w/v) (*i.e.*, 0.025, 0.25 and 1.0) of Pt-salt (Chloroplatinic acid Hexahydrate ($H_2PtCl_6 \cdot 6H_2O$), Sigma-Aldrich, USA) separately. The films were deposited through a solution-casting process on clean glass substrates. The as-cast films were subsequently dried at 120°C for 5 h. The free-standing films (thickness: $\sim 10 - 15\ \mu m \pm 4\ \mu m$) were indexed as NeatPVF₂ (where no additive is present) and PVF₂Pt#, where # stands for the different concentration (w/v-%) of Pt-salt with respect to PVDF-DMF solutions.

Characterization. To examine the *in-situ* formation of Pt-NPs and relevant crystalline modification in PVDF, the X-ray diffraction (XRD) analysis was performed by X-ray diffractometer (Bruker, D8 Advance) with CuK_{α} X-ray radiation ($\lambda = 0.154178\ nm$). The optical properties were studied with UV-Vis spectrometer (Shimadzu, 3110PC). For better comparison

UV-Vis spectra were normalized with corresponding film thickness. The optical microscopy (Leica, DM750P) images were taken to check the surface morphologies as well as birefringence effect by operating in unpolarize ($A \parallel P$) and polarize ($A \perp P$) modes respectively. The Field Emission Scanning Electron Microscopy (FE-SEM, FEI, INSPECT F 50) images were recorded to investigate the detail surface morphological features. For elemental chemical component analysis, Energy Dispersive X-ray Spectroscopic (EDS) were recorded with Bruker Nano X-flash detector (410-M), equipped with FE-SEM chamber. The characteristic vibrational modes (which are also related to crystalline modification of PVDF) present in PVDF were analysed by Fourier Transform Infrared Spectroscopy (FT-IR, Shimadzu, 8400S), where 8 cm^{-1} spectral resolution and 100 number of scans were applied. The tactile sensors were prepared by simply pasting the carbon tape as electrodes on both sides of the films. The human finger touch responses were recorded (ESI, Video S1) in terms of output voltage (Agilent DSO3102A) from tactile sensors through typical bridge circuit (ESI, Fig. S10). The Photoluminescence (PL) spectra of the Pt-NPs doped PVDF films under the excitation wavelength of 260 nm were recorded using Horiba (iHR320) luminescence spectrometer.

RESULTS AND DISCUSSION

The XRD pattern, as exhibited in Fig. 1 is the obvious indication of the *in-situ* formation of metallic platinum and its doping in PVDF films. The peaks appeared at 39.9° , 46.5° , 67.8° and 81.6° in $\text{PVF}_2\text{Pt}1.0$ film corresponds to the diffraction from (111), (200), (220) and (311) lattice planes of fcc-Pt [$Fm\bar{3}m$ (225)] as per the JCPDS card no.04-0802. Likewise, two intense diffraction peaks [*i.e.*, (111) and (200)] are also present in $\text{PVF}_2\text{Pt}0.25$ and $\text{PVF}_2\text{Pt}0.025$ films as well. Nevertheless, the diffraction from (220) and (311) lattice planes are not appeared in these two films. It is also interesting to note that, especially in $\text{PVF}_2\text{Pt}1.0$ film, the relative intensities

of the (200) and (220) peaks are very close to the 'bulk', however, the relative intensity of (311) peak is considerably high (~10 %). In contrast, the relative intensities of (200) peak in PVF₂Pt0.25 and PVF₂Pt0.025 films are noticeably low. This result indicates that the PVF₂Pt1.0 film is rich of {220} and {311} facets, rendering it of high interest for catalytic applications.⁸

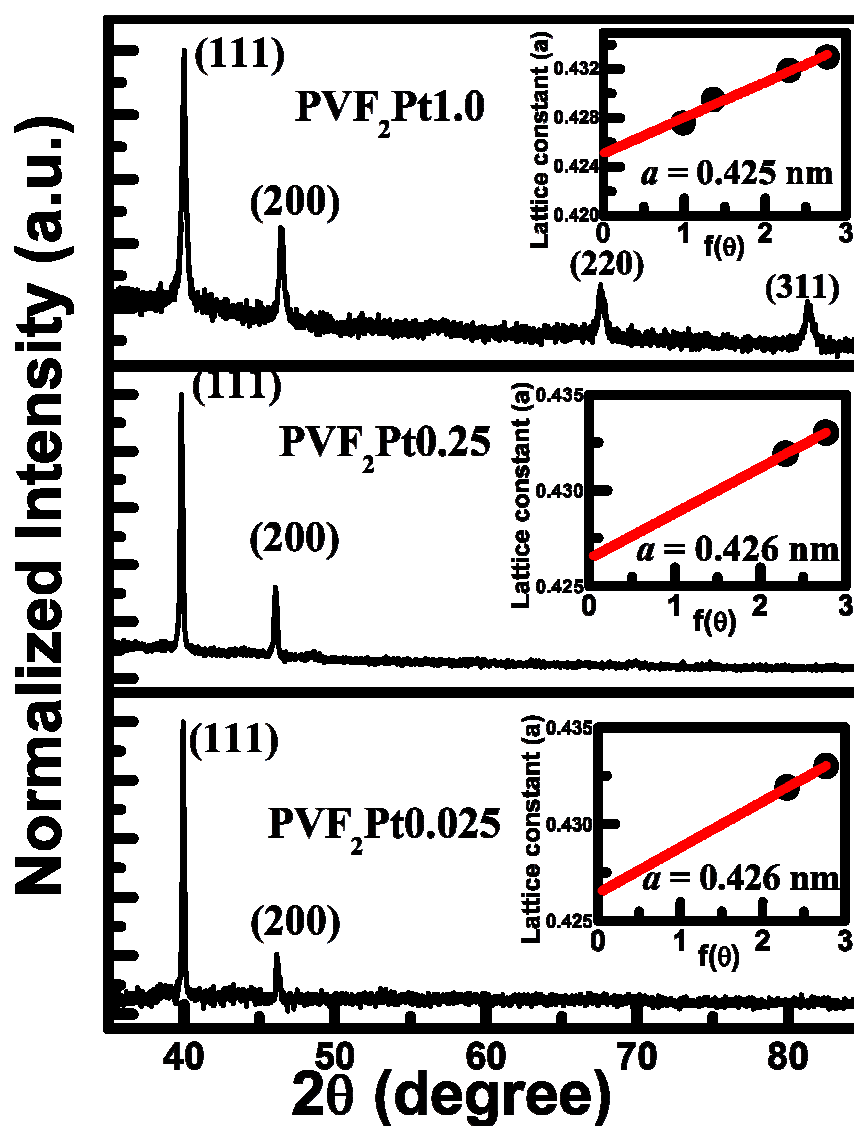


Fig. 1 XRD pattern of Pt-NPs doped PVDF films where $2\theta = 35$ to 85° region is shown for indexing the diffraction peaks from Pt-NPs and inset figures show the Nelson- Riley plot of the respective films.

The XRD result also indicates that geometrical environment of PVDF may cause to change the electronic structure of Pt-NPs.²³ The selective interaction of the counter part of PVDF (*i.e.*, chain conformation and crystallinity) with different crystal planes of Pt-NPs may also affect the growth rates and thus the diffraction the intensity of the different crystal planes of Pt-NPs. The average size of Pt-crystallites is calculated by using the Debye–Scherrer equation: $D = \frac{k\lambda}{\beta \cos \theta}$

(1) Where, K is a constant (0.89), λ is the wavelength (0.154178 nm) of the X-ray radiation, β is the full-width (in radian) at half-maximum (FWHM) of the intense diffraction peak, θ is the angle of diffraction. It gives the average crystallites size of Pt in the (*i.e.*, ~ 61 nm in PVF₂Pt1.0, ~ 82 nm in PVF₂Pt0.25 and ~ 97 nm in PVF₂Pt0.025 film) nano-dimensional range. The lattice constant (*a*) of Pt-nanocrystallites in doped PVDF films is estimated (*a* = 0.425 nm) from the intercept of the Nelson-Riley plot [shown in inset of Fig. 1] with error function $f(\theta) = \frac{1}{2} \left(\frac{\cos^2 \theta}{\sin \theta} + \frac{\cos^2 \theta}{\theta} \right)$.

The photographs of the Pt-NPs doped PVDF films are quite transparent (Fig. 2a) and the transparency is reduced with the increasing density of Pt-NPs. This observation consistently matched with the transmittance spectra provided with the photograph of the films. The adequate flexibility of the Pt-NPs doped PVDF films is presented in Fig. 2b, where any undesirable micro cracks are not detectable. Furthermore, Pt-NPs doped PVDF films showing relatively larger absorbance in the UV region and a broad band appeared around 270 nm as depicted in Fig. 2c, indicates the absence of [PtCl₆]²⁻ ions and the full conversion of Pt-metallic (Pt⁰) states (ESI, Fig. S1).²⁴ The increasing trend of absorbance with concentration of Pt-salt indicates the increasing gradient of Pt-NPs formation. Therefore, the presences of Pt-NPs in PVDF films, as observed from XRD results are consistent with this observation. Besides this, the intense and a broad

absorption features in the UV- region attributed to the strong *d-sp* interband transition comprising from Pt-NPs.^{14,25} As a consequence, the degree of UV- absorbance (ESI, Fig. S2) undergoes a sharp improvement due to Pt-NPs doping as revealed in the inset of Fig. 2c.

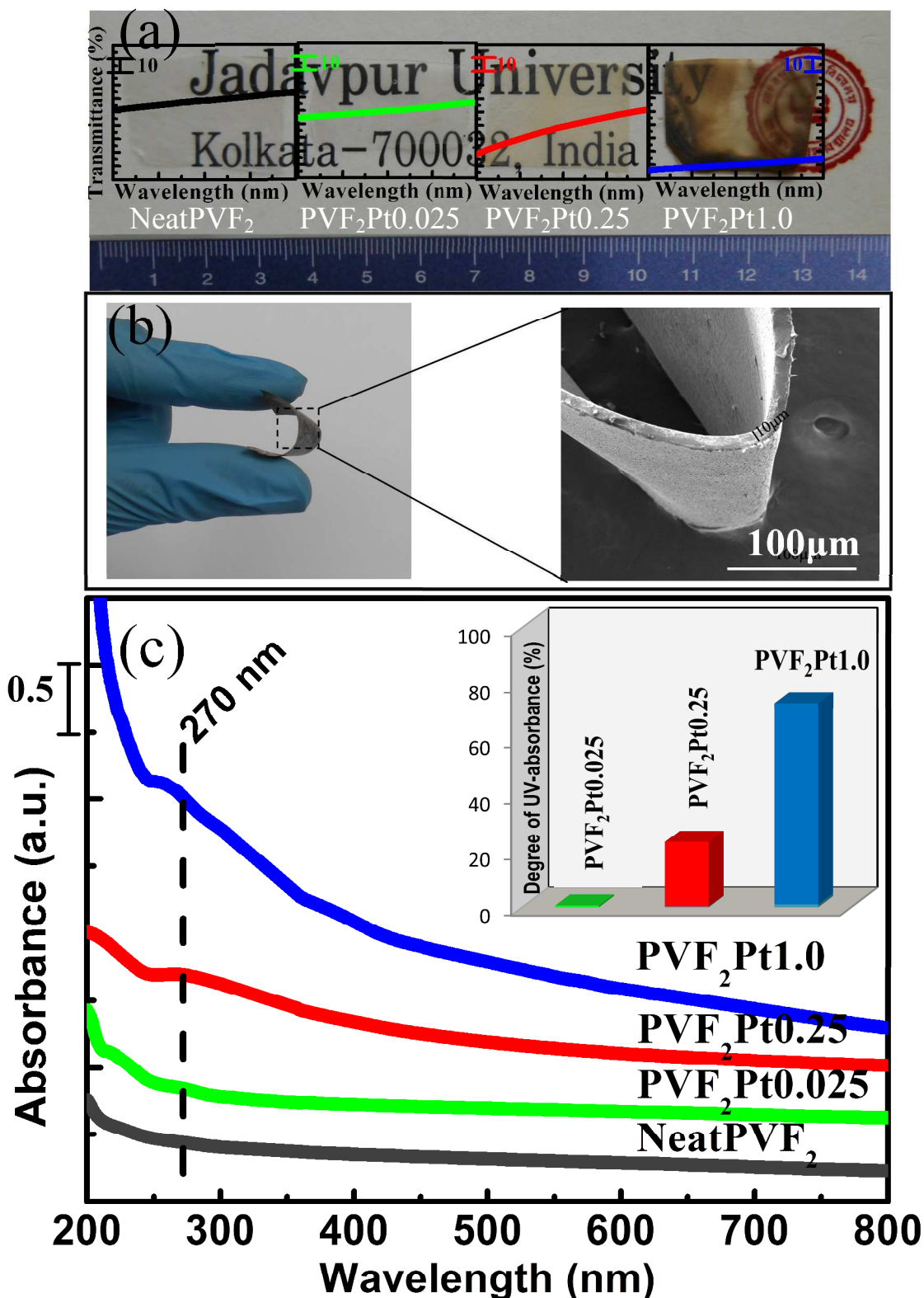


Fig. 2 (a) Spectral transmittance (in visible region: 400-800 nm) and digital photograph of NeatPVF₂ and Pt-NPs doped PVDF films, (b) Superior flexibility of Pt-NPs doped PVDF (sample: PVF₂Pt1.0) film is shown by digital photograph (left panel) and FE-SEM image (right panel), (c) UV-Vis absorbance spectra of NeatPVF₂ and Pt-NPs doped PVDF films (for clarity, absorbance of each spectrum are shifted arbitrarily). The Degree of UV-absorbance of Pt-NPs doped PVDF films is illustrated in the inset.

The optical microscopic (OPM) images with cross-polarize view (inset images) of NeatPVF₂ and Pt-NPs doped PVDF films are shown in Fig. 3 (a~d). The images demonstrate that the small hump like structures over the surface of NeatPVF₂ film (Fig. 3a) and these are atrophied tardily in Pt-NPs doped PVDF films (Fig. 3b~d). Interestingly, the directional fiber layers over PVDF surface are observed in PVF₂Pt1.0 film (Fig. 3d) due to the influence of larger proportion of Pt-NPs in PVDF film (ESI, Fig. S3). On the other hand polarized optical microscopic (POM) images ($A \perp P$) presented in the inset of Fig. 3(a ~ c) exhibit the presence of spherulitic feature that usually arises due to presence of linear optical anisotropy (birefringence effect) occur in $TGT\bar{G}$ (α -phase) and $T_3GT_3\bar{G}$ (γ -phase) orientations. The strong birefringent effect comprising from large spherulites ($\sim 25 \mu\text{m}$ of average diameter) of compact and well-defined structure with Maltese-cross texture (shown by dotted lines in the inset of Fig. 3a) describe the predominant presence of α -crystalline phases in NeatPVF₂ film.²⁶ Commonly, these spherulitic growths are originated from the nucleus and their radial growths with clear boundaries are observed in NeatPVF₂ film. These boundaries are due to the encroachment of spherulites. The OPM images

of PVF₂Pt0.025 and PVF₂Pt0.25 films (inset of Fig. 3b and c) indicate the decreasing nature of large, strong α -spherulites and increasing tendency of relatively small, weakly birefringent

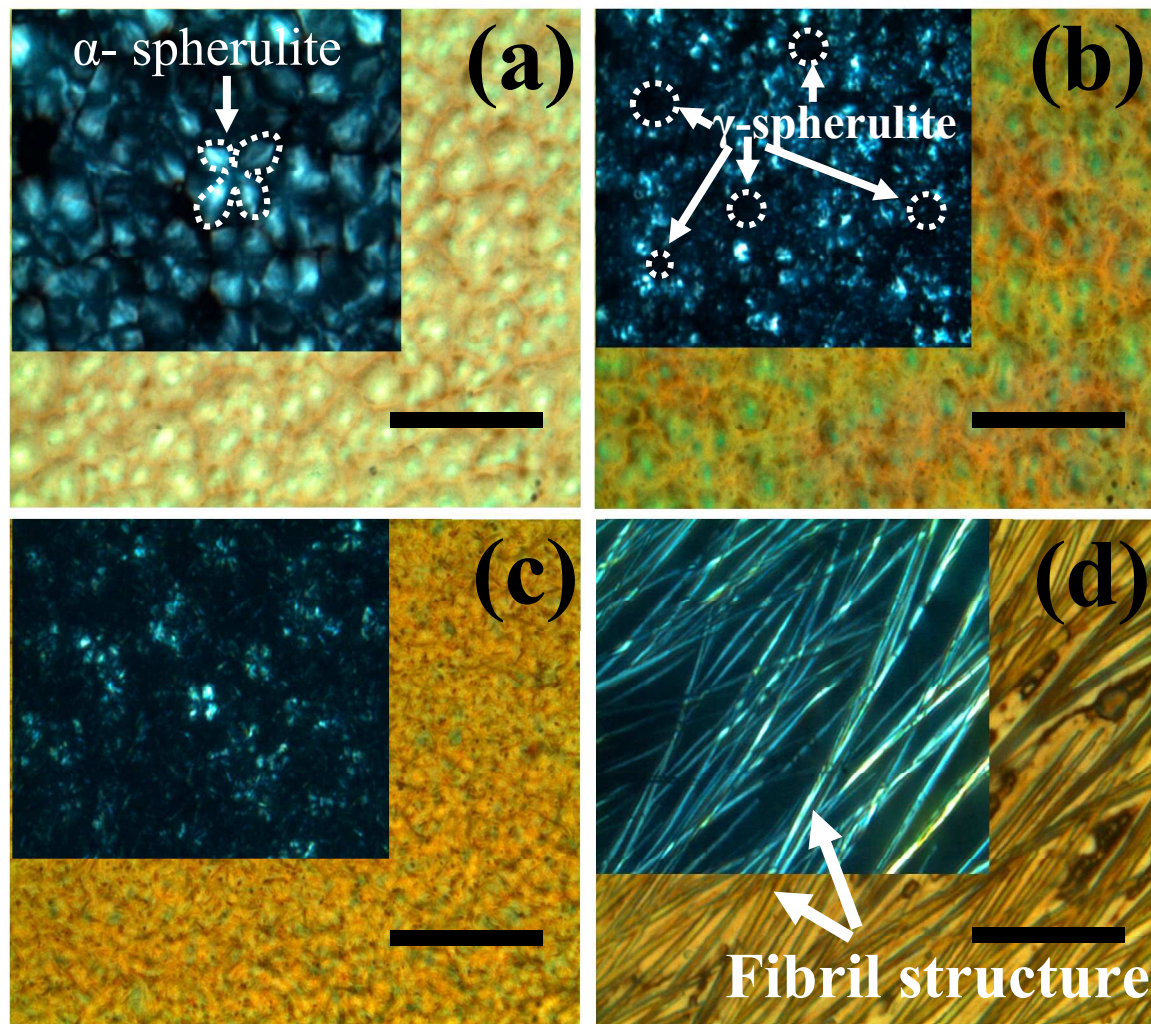


Fig. 3 Optical microscopic images of (a) NeatPVF₂, (b) PVF₂Pt0.025, (c) PVF₂Pt0.25, and (d) PVF₂Pt1.0 films. The unpolarize (A||P) and cross polarize (A⊥P) (inset figures) views are shown in same scale bar: 50 μ m.

spherulites which is the characteristic of γ -crystal (shown by dotted circles in inset of Fig. 3b). Thus the diminishing tendency of α -spherulites and subsequent appearance of γ -spherulites in Pt-NPs doped PVDF films imply that there may also exist β -spherulites which does not show

optical anisotropy in polarizing optical microscopy images due to the weak birefringence nature.²⁷ In contrast, PVF₂Pt1.0 film does not represent any typical α - or γ -spherulites but the fibril like structure (obtained in unpolarized mode, Fig. 3d) shows the significant anomaly birefringent effect (depicted in the inset of Fig. 3d), probably due to the large difference of refractive index (optical anisotropy) comprising from the Pt and PVDF surfaces. The intense variation of the Pt-PVDF fibril structure probably hindered the view of typical γ -spherulitic structure in the surface of the film, if any.

The detail surface morphology of NeatPVF₂ and Pt-NPs doped PVDF films are examined through FE-SEM images depicted in Fig. 4(a~d). The typical fibril growth of α -spherulite (marked by arrow, Fig. 4a) is mainly observed on NeatPVF₂ surface, whereas it remarkably diminishes in Pt-NPs doped PVDF films. In PVF₂Pt0.025 film, a trace amount of α -spherulite (marked by dotted boundary, Fig. 4b) is appeared, however, it is completely diminishes in PVF₂Pt0.25 and PVF₂Pt1.0 films. Nevertheless, Pt-NPs are uniformly distributed over the surface of PVF₂Pt0.025 film as shown through the enlarge view of the FE-SEM image (inset of Fig. 4b). In contrast, quite different surface morphologies are observed in PVF₂Pt0.25 and PVF₂Pt1.0 films, indicating the significant effect of *in-situ* formation of Pt-NPs when concentration of Pt-salt increases. PVF₂Pt0.25 film (Fig. 4c) exhibits the anisotropic distribution of Pt-nanoclusters (NCs) strips embedded within the PVDF surface (in Fig. 4c, few Pt-NCs strips are marked by arrows and a schematic diagram of one Pt-NCs strip has been cited). In addition, the presence of uniform Pt-NPs are also observed over the entire surface (in the inset of Fig. 4c) along with the random distribution of Pt-NCs strips. Furthermore, Pt-NCs strips are lengthy and quite well arranged (indicated by arrows in Fig. 4d) in PVF₂Pt1.0 film, few well arranged Pt-NCs strips are marked with dotted lines. The enlarged view of the selected area in PVF₂Pt1.0 film

(demonstrate the inset of Fig. 4d) indicates that quite well disperse Pt-NPs are also present in between the region of Pt-NCs strips. The presence of Pt-NPs was further evidenced from energy dispersive X-ray spectroscopic (EDS) spectrum (ESI, Fig. S4). The presence of C and F due to

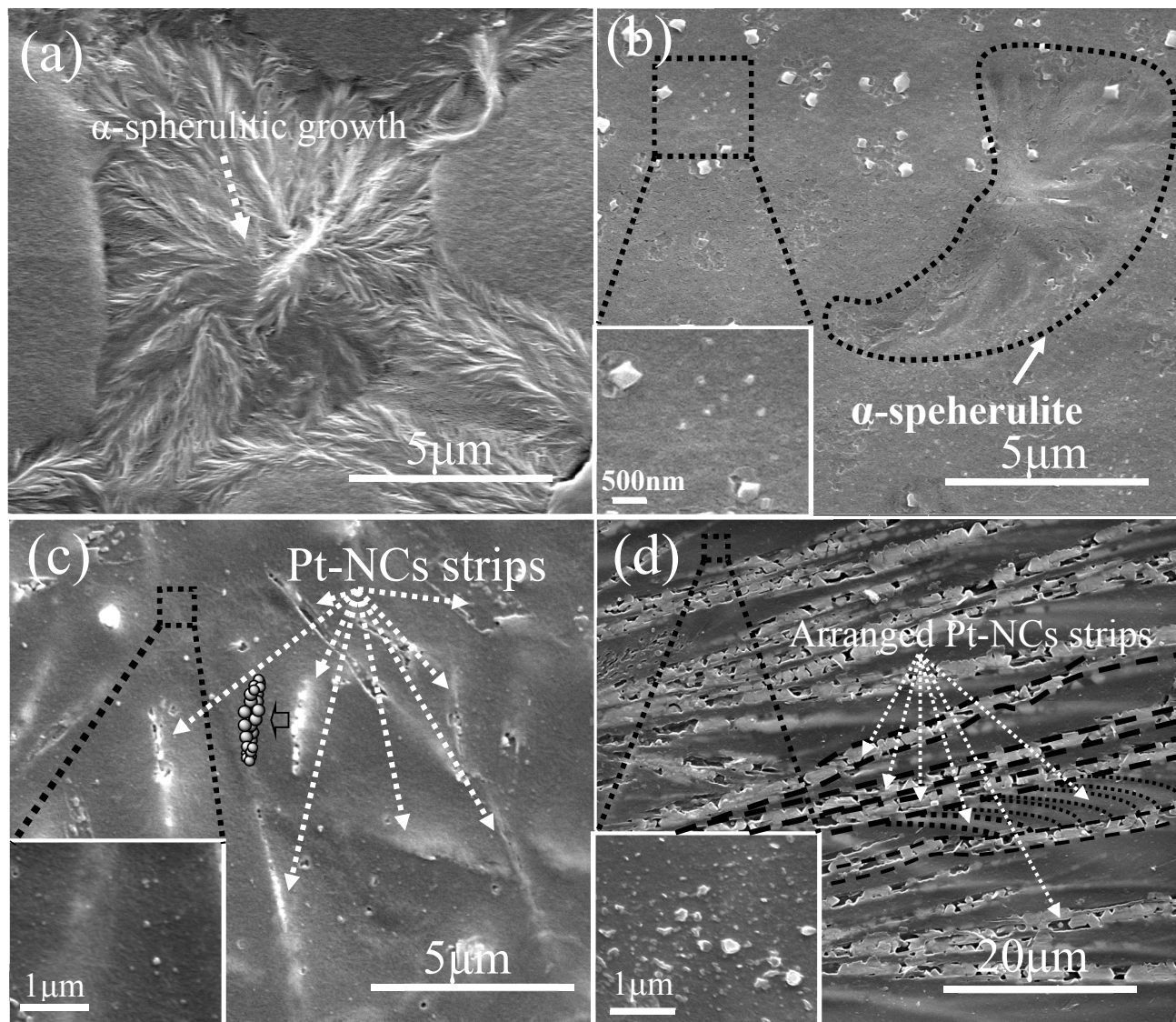


Fig. 4 FE-SEM images of (a) NeatPVF₂, (b) PVF₂Pt0.025, (c) PVF₂Pt0.25, and (d) PVF₂Pt1.0 films. In inset, the enlarge view of the selected region of the respective images are shown.

PVDF and Pt due to NPs formation were well detected in the EDS spectrum. Thus it is self-evident that the surface morphology can be tuned by simply changing the concentration of the Pt-salt. As this large variation of the surface morphology is solely depend on the size, shape, and distribution of Pt-NPs over PVDF surface, so it indicates that Pt-NPs doped PVDF films may have versatile functionalities for chemical sensor applications.²⁸

The FT-IR spectra of NeatPVF₂ as well as Pt-NPs doped PVDF films are shown in Fig. 5a and corresponding vibrational bands are labeled as per the presence of crystalline phases. It exhibits NeatPVF₂ film predominantly composed of α -crystalline phase attributing from the strong absorption peaks at 1211, 1150, 976, 856, 796, 764, 613 and 532 cm⁻¹.²⁹ In contrast, Pt-NPs doped PVDF films illustrate two additional intense peaks arise at 1277 and 1234 cm⁻¹ are due to the nucleation of the β and γ -phases respectively.^{4,9,29} Few α -characteristic vibrational bands at 976, 796, 764, 532 cm⁻¹ are still appeared in PVF₂Pt0.025 film, indicates 0.025 wt% of Pt-salt is not sufficient to hinder the α -crystalline growth completely. Nevertheless, the improvement of the intensity of 841 cm⁻¹ and clear appearance of 1277 as well as 1234 cm⁻¹ bands indicate that the nucleation of the electroactive β and γ -phases takes place even with the trace amount of Pt-NPs prepared from 0.025 wt% (0.048 mM) of Pt-salt. Furthermore, PVF₂Pt0.25 film exhibits the complete removal of the non-polar α -characteristic phase and complete conversion of the electroactive counterpart of PVDF. Some occurrences are observantly kept in view that if we increase the concentration of Pt-salt gradually in PVDF matrix, then further improvement of the β and γ -band intensity has also been notified (ESI, Fig. S5). It is mentionable that for the qualitative analysis of the α , β and γ -phases the absorbance is normalized at 1072 cm⁻¹ band as it

has a linear dependence with the film thickness regardless of crystalline modification.⁵ The absorption intensity ratio of β (I_{1277}) and α (I_{764}) -phases, *i.e.*, I_{1277}/I_{764} in NeatPVF₂ and Pt-NPs

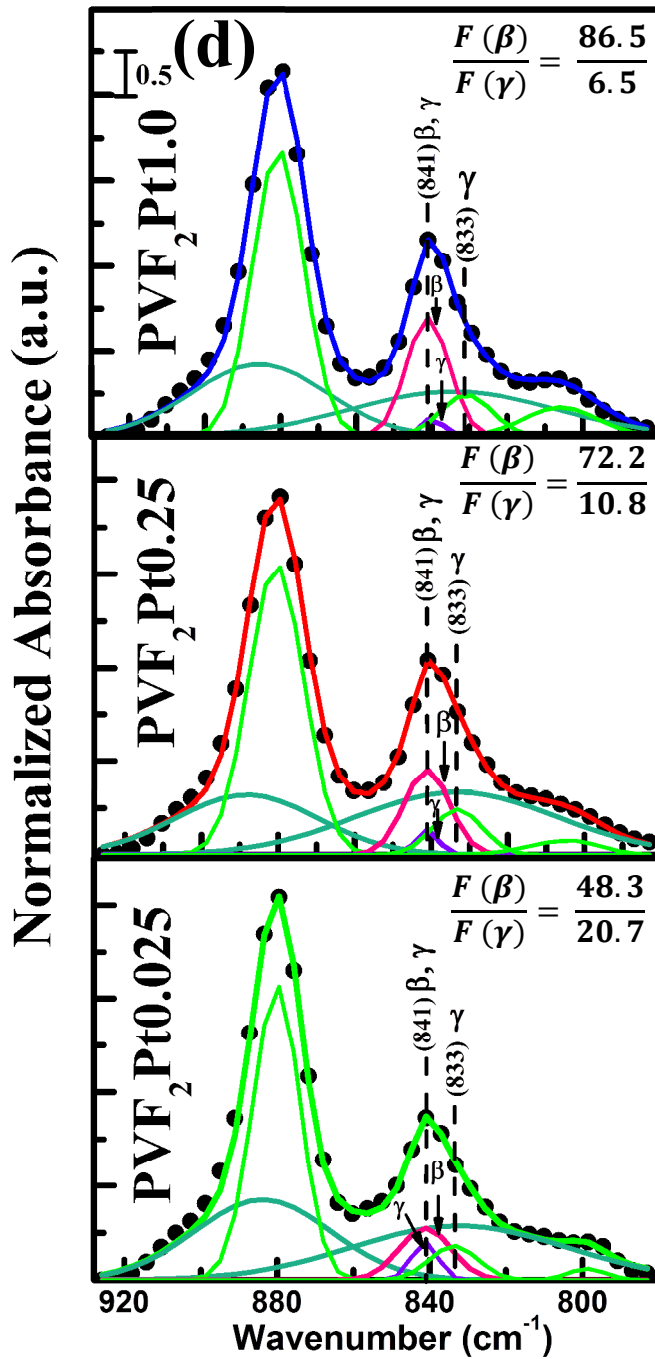
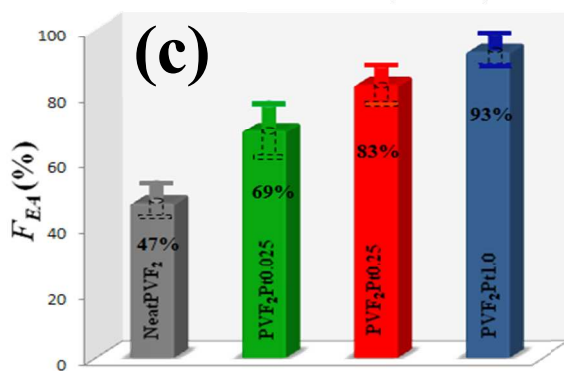
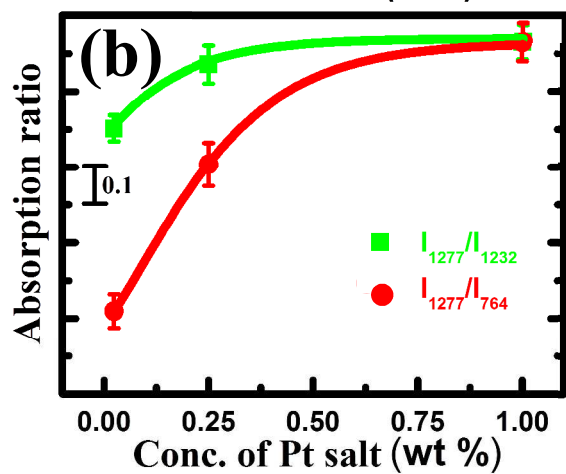
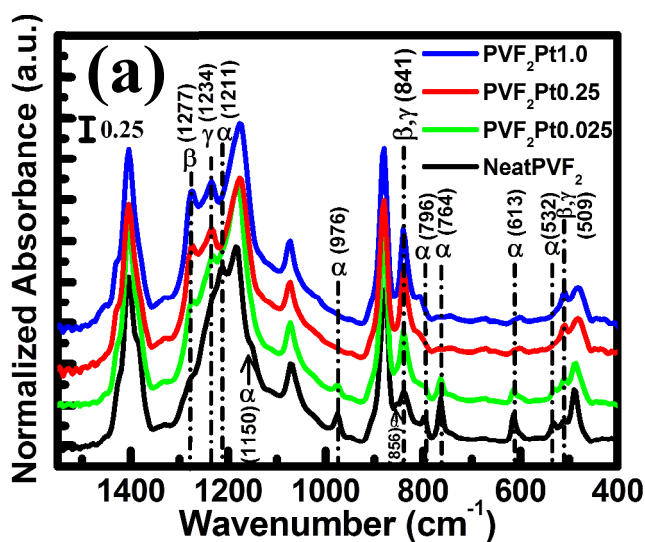


Fig. 5 (a) FT-IR spectra of NeatPVF₂ and Pt-NPs doped PVDF films in 1550 – 400 cm⁻¹ frequency region, (b) Dependence of the absorption ratio of β and α -phases (I_{1277}/I_{764}) as well as β and γ -phases (I_{1277}/I_{1234}) of Pt-NPs doped PVDF films with concentration of Pt-salt from FT-IR spectra are shown, (c) The percentage of F_{EA} for NeatPVF₂ and Pt-NPs doped PVDF films, (d) The deconvolution of the FT-IR spectra (920-780 cm⁻¹) of Pt NPs doped PVDF films is shown. The dotted points are experimental data and the solid from the best curve fit. The ratio of $F(\beta)$ and $F(\gamma)$ are mentioned in the inset.

doped PVDF films is depicted in Fig. 5b, reveals that it gradually increases as the concentration of Pt-salt (*i.e.*, also Pt-NPs) increases and reached maximum (*i.e.*, $I_{1277}/I_{764} = 0.93$) in PVF₂Pt1.0 film. It is interestingly noticeable that even though the PVF₂Pt0.25 film does not exhibit the α -characteristic bands (Fig. 5a), however I_{1277}/I_{764} is far below from its maximum, observed in PVF₂Pt1.0 film. This is significantly pointed out that PVF₂Pt0.25 film has large amount of additional contribution other than the β -phase, *i.e.*, the γ -phase, as evident from the relatively intense 1234 cm⁻¹ band (Fig. 5a). It is noteworthy to mention that as NeatPVF₂ film predominately consists of α -phase, therefore for comparison, the contribution from the β and γ -phases is not taking into account for further analysis. The absorption intensity ratio of β (I_{1277}) and γ (I_{1234})-phases *i.e.*, I_{1277}/I_{1234} is also demonstrated in Fig. 5b, indicates the hindering of γ -crystalline growth when the concentration of Pt-NPs is increased gradually. Thus it seems that PVF₂Pt0.25 and PVF₂Pt1.0 films contain a large proportion of the β -phase.

It is to be mentioned that the 841 cm⁻¹ band strongly appeared in Pt-NPs doped PVDF films (Fig. 5a), is common characteristic of electroactive β and γ -phases.^{4,9,29,30} Thus the absorption intensity at 841 cm⁻¹ band can be assigned to quantify the relative proportion of electroactive phases (*i.e.*,

F_{EA}) attributing to both β and γ -phases. The F_{EA} is related with the eq. (2) as follows,

$$F_{EA} = \frac{I_{EA}}{\left(\frac{K_{841}}{K_{764}}\right)I_{764} + I_{EA}} \times 100\% \quad \dots\dots\dots (2) \quad \text{Where, } I_{764} \text{ and } I_{EA} \text{ are the absorbance}$$

intensity at 764 and 841 cm^{-1} respectively; K_{764} and K_{841} are the absorption coefficients at the respective wave numbers.²⁶

One important consequence of equation 2 has been noted, as the rapid growth of electroactive phase (F_{EA}) formation with increasing amount of Pt-precursor (Fig. 5c) up to 1.0 wt% of Pt-salt concentration has been occurred and then slowly improved up to 99 % of F_{EA} (ESI, Fig. S6). The quantification of individual β and γ -phases is also performed by curve deconvolution of 841 cm^{-1} band (shown in Fig. 5d), where the broadening contribution due to γ -phase and sharp well resolved peak for β -phase has been considered.³⁰ The equations of (3a) and (3b) are used to quantify the relative proportion of electroactive β and γ -phases individually.

$$F(\beta) = F_{EA} \times \left(\frac{A_{\beta}}{A_{\beta} + A_{\gamma}}\right) \times 100\% \quad \dots\dots\dots (3a)$$

$$F(\gamma) = F_{EA} \times \left(\frac{A_{\gamma}}{A_{\beta} + A_{\gamma}}\right) \times 100\% \quad \dots\dots\dots (3b)$$

Where, A_{β} and A_{γ} are the integrated area under the β and γ marked deconvoluted curves (shown in Fig. 5d) respectively, centered at 841 cm^{-1} band. The ratio of $F(\beta)$ and $F(\gamma)$ depicted in the inset of Fig. 5d, offering the large content of relative proportion of β -phase than the γ -phase in Pt-NPs doped PVDF films. Thus, it is manifested that Pt-NPs doped PVDF films comprising of large amount (*i.e.*, 69 % to 99 %) of electroactive β and γ -phases and also relative proportion of β -phase promising highly suitable for piezo-, pyro- and ferro-electric based sensors, actuators and also for vibration based energy harvesters.^{31,32}

These results emphasize on the fact that Pt-NPs play a significant catalytic role for nucleating the piezoelectric β -phase and subsequent stabilization. This can be interpreted by the surface charge (of NPs) and dipoles (of PVDF) interaction model as thought previously.⁴ A clear frequency shifting of the CH₂ asymmetric (ν_{as}) and symmetric (ν_s) stretching vibrational modes are observed (Fig. 6a) in Pt-NPs doped PVDF films in comparison with NeatPVF₂ film, is the indication of the interfacial interaction causes from the surface charge of the Pt-NPs (σ_{eff}^+) and CH₂ (also CF₂) dipoles (δ_{eff}^-) of PVDF.

Recently, for clarifying this type of interfacial interaction, a damping constant ($2r_{dc}$) associated with the frequency of CH₂ vibration (ν -CH₂) is proposed by considering the frequency shift from the NeatPVF₂ film.³³ It has been assumed that the effective mass of CH₂ dipoles is increased due to the interfacial interaction. As a result a damping may occur; this decreases the vibrational frequency (*i.e.*, wavenumber) of the CH₂ stretching vibration. The damping constant ($2r_{dc}$) is related to the wavenumber ($\bar{\lambda}_{int}$) of CH₂ stretching vibration (ν -CH₂) due to damped oscillation for Pt-NPs doped PVDF films as,

$$\bar{\lambda}_{int} = \left[\bar{\lambda}_0^2 - \left(\frac{r_{dc}}{2\pi c} \right)^2 \right]^{1/2} \dots\dots\dots (4)$$

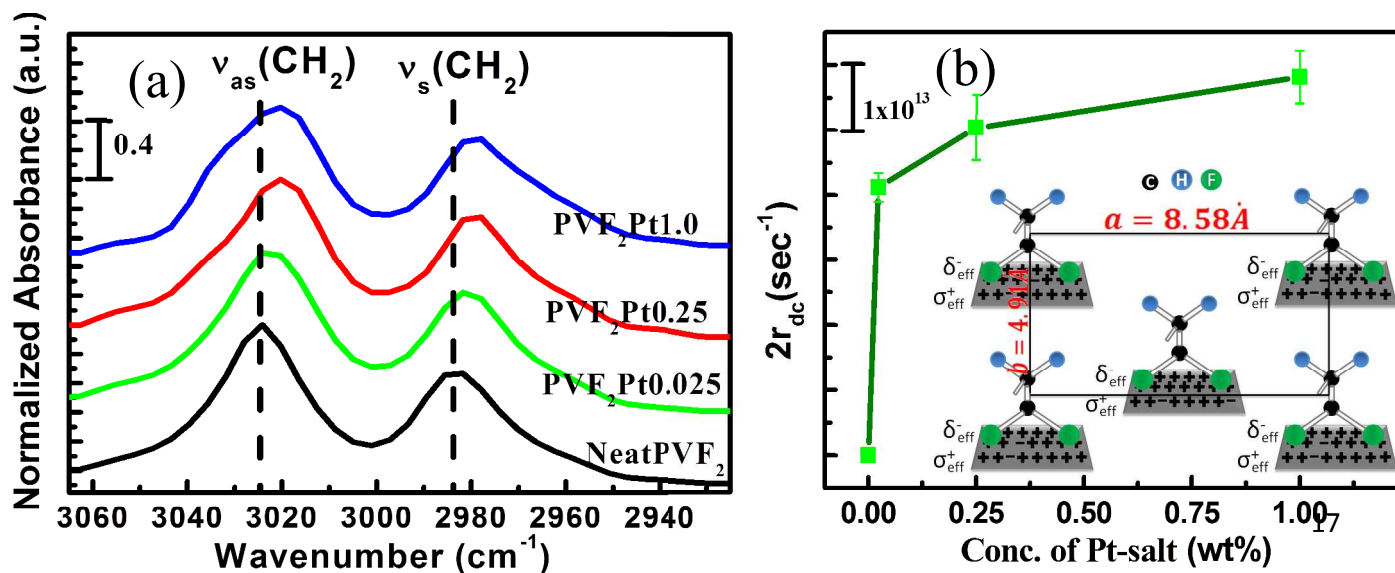


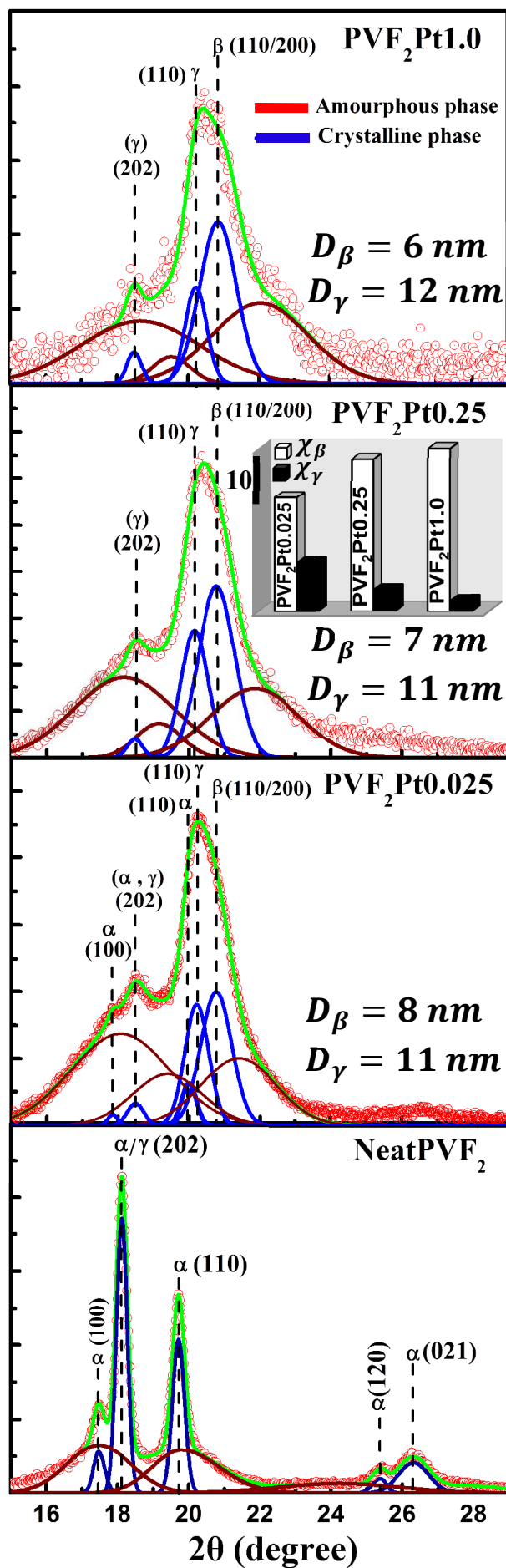
Fig. 6 (a) FT-IR spectra of NeatPVF₂ and Pt-NPs doped PVDF films in 3060 – 2940 cm⁻¹ region; (b) Variation of damping coefficient ($2r_{dc}$) as function of concentration of Pt-salt. The inset shows the unit cell of β -phase, where the interfacial interaction between the surface charge of Pt-NPs (assuming the effective positive surface charge density of nano-particles *i.e.* σ_{eff}^+) and CF₂ dipoles (δ_{eff}^-) are illustrated.

Where, $\bar{\lambda}_0$ is the wavenumber of ν -CH₂ in damping free vibration, occur in NeatPVF₂ film and $\bar{\lambda}_{int}$ are the corresponding wavenumber due to damped vibration possess Pt-NPs doped PVDF films; c is the velocity of the light. Fig. 6b shows that damping constant $2r_{dc}$ increases asymptotically as a function of Pt-NPs loading in PVDF matrix. Thus the increase of $2r_{dc}$ value indicates the improvement of interfacial interaction which improves β -phase content. The inset of Fig. 6b represents a unit cell of β -phase, where the interfacial interaction is represented.

Crystallinity of the NeatPVF₂ and Pt-NPs doped PVDF films are evaluated from the XRD pattern by curve deconvolution technique, demonstrated in Fig. 7. NeatPVF₂ film exhibits the diffraction peaks at 17.6°(100), 18.2°(202), 19.7°(110), 26.2°(021) and a shoulder at 25.4° (120) are the characteristic of α -crystalline phase.^{11,27} Thus NeatPVF₂ film consists of predominantly α -crystalline phase which is consistent with FT-IR spectra as shown in Fig. 5a. Apparently, PVF₂Pt0.025 film shows the α -phase attributing from 17.6° (100) and 18.5° (202) diffraction peaks. Moreover, the diffraction peak at 18.5° (202) in Pt-NPs doped PVDF films is attributing the presence of the γ -phase as the α -characteristic peak at 17.6° is absent. Likewise, the main intense diffraction peak at 20.5° is the dual signature of the β and γ phases²⁷ that needs curve deconvolution to resolve the individual contribution. Applying deconvolution method, the presence of β -phase at 20.8° (110/220) and γ -phase at 20.2° (110) are classified individually.

The degree of crystallinity (χ_c) is calculated from $\chi_c = \frac{\sum A_{cr}}{\sum A_{cr} + \sum A_{amr}} \times 100\%$ (5), where $\sum A_{cr}$ and $\sum A_{amr}$ are the summation of integral area of crystalline peaks and amorphous halo respectively. It indicates that the overall crystallinity of Pt-NPs doped PVDF films has been changed remarkably as the concentration of Pt-salt increases (ESI, Table S7), which is one of the common observations in polymer nanocomposites, also suitable for improving the dielectric properties.³⁴ In addition, these reductions of χ_c does not affect the electroactive properties of PVDF as the piezoelectric β -phase content is increased (ESI, Table S8) significantly. As a consequence, the large crystallite size (depicted in inset of Fig. 7) of β (D_β) and γ (D_γ) crystallite (calculated from Debye–Scherrer equation as mentioned in equation 1) assists the molecular (*i.e.* CH₂ or CF₂) dipoles to be more co-operative to give higher ferroelectric responses.³⁵ Thus, these Pt-NPs doped PVDF films promising to have better ferroelectric properties (ESI, Fig. S9) in addition of its superior piezoelectric phenomena as per its enhanced piezoelectric phase content (ESI, Table S8) is concern. Reproducing the repeating proprioceptive human finger touch has been demonstrated in terms of piezo-response from tactile sensor fabricated with Pt-NPs doped PVDF films shown in Fig. 8. It illustrated that piezo-response has been considerably improved in Pt-NPs doped films compared to Neat PVDF. It exhibited the pulse rectified output (ESI, Fig. S10), represents the corresponding selective finger touch and release response. The piezosensitivity (in terms of output voltage) is considerably enhanced in Pt-NPs doped PVDF films in comparison with NeatPVF₂ film. This is probably the improved electrostriction effect in Pt-NPs doped electroactive PVDF films. As the local polarization is compensated by space charges at the end of the crystallites and each amorphous void behaves like a spring. Thus, the difference in the relative size of the force constants of the voids develop a potential difference between the opposite surfaces of the films resulting an enhance output voltage.³⁶

Intensity (a.u.)



RSC Advances Accepted Manuscript

Fig. 7 The curve deconvolution of XRD pattern in $16\text{-}28^\circ$ (2θ) range of NeatPVF₂ and Pt-NPs doped PVDF films. The degree of β and γ -crystallinity is depicted within the inset fig. and corresponding crystallite size (D_β and D_γ) is also mentioned.

Therefore, the output voltages of these films (ESI, Fig. S11) are not as symmetrical as typically found in normal piezo-electric nanogenerators (NGs).³³ Furthermore, the high output voltage generation and tremendous touch sensitivity (ESI, Video S1) from unpoled Pt-NPs doped PVDF films signifying the great potential feasibility to develop energy harvester which is expected to be a future power source for next generation portable electronic devices.³⁷ Furthermore, upon electrical poling, it is also expected that high piezoelectric β -phase containing Pt-NPs doped PVDF films will exhibit considerably high piezoelectric output, probably ideal for flexible nanogenerator fabrication or self-charging battery separator.³⁸

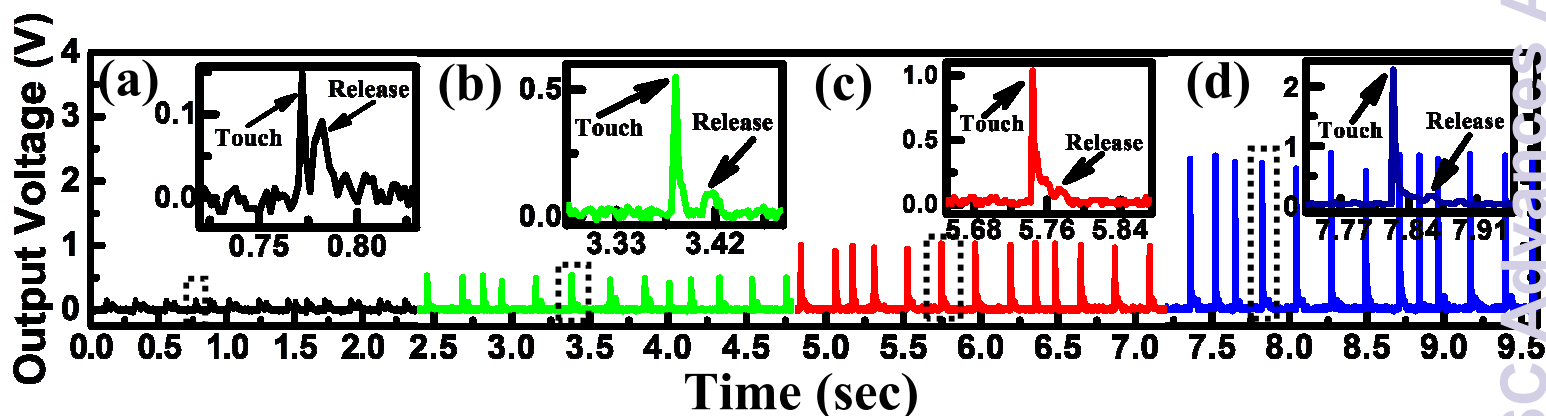


Fig. 8 Finger touch response (rectified output voltage) from (a) NeatPVF₂, (b) PVF₂Pt0.025, (c) PVF₂Pt0.25 and (d) PVF₂Pt1.0 films at room temperature. The insets show the enlarge view of one selected peak responsible for press and release of gentle finger touch (ESI, Fig. S11 and ESI Video S1).

The room temperature PL spectra illustrated in Fig. 9(A), exhibit the intense broad UV-emissions from UV-B to UV-A regions in Pt-NPs doped PVDF films. It attributes to the fact that Pt-NPs act as an important role for generating UV-emission as there is a forbidden emission in NeatPVF₂ film (ESI, Fig. S12). Deconvolution of the PL-spectrum indicates that each of the emission spectra is composed of mainly three Gaussian curves, viz. B, A₁ and A₂ curves (mentioned in Fig. 9A). The A₁ and A₂ curves belong to UV-A region, whereas curve B belongs to UV-B region. The resultant contribution of B and A₂ curves, revealed from their integrated areas, is more pronounced than that of the A₁ curve with the lower concentration of Pt-NPs doped in PVDF matrix. The overall broad emission indicates that the Pt-NPs doped PVDF films have good luminescence quality. It is also observed that UV-emission peaks are shifted towards the lower wavelength with increasing concentration of Pt-NPs (ESI, Fig. S13). This might be due to the formation of Pt-NCs, observed in PVF₂Pt0.25 and PVF₂Pt1.0 films (Fig. 4c and 4d).^{39,40} It has been found that the frequency of the Localized Surface Plasmon Resonance (LSPR) can be tuned by changing the size, shape, and dielectric constant of the surrounding medium for a given metal-dielectric combination.⁴¹ Theoretically, it has been established that noble metals give rise the PL due to the direct recombination of the conduction-band electrons near the Fermi level with the holes in the *d*-band.⁴² Thus, the entire photo excitation and emission can be explained by the schematic illustrated in Fig. 9B (i). Initially, the *d*-band electrons lead to interband transitions by absorbing the incident photons [Fig. 9B (i)]. The energy required to promote these electrons from the filled *d*-band to the unoccupied *sp*-conduction band above the Fermi level is supplied by the photon energy (*hν*). Both the electrons and holes can relax by scattering with phonons then recombine radiatively to produce the emission. But this interband transition only

involved the visible emission from metal NPs⁴² which is forbidden in Pt-NPs doped PVDF film. It should also be noted that to data very few reports are available where intense visible luminescence is observed for Pt-NPs.^{17, 43} In contrast, UV-emission from the Pt-NPs is not reported yet.

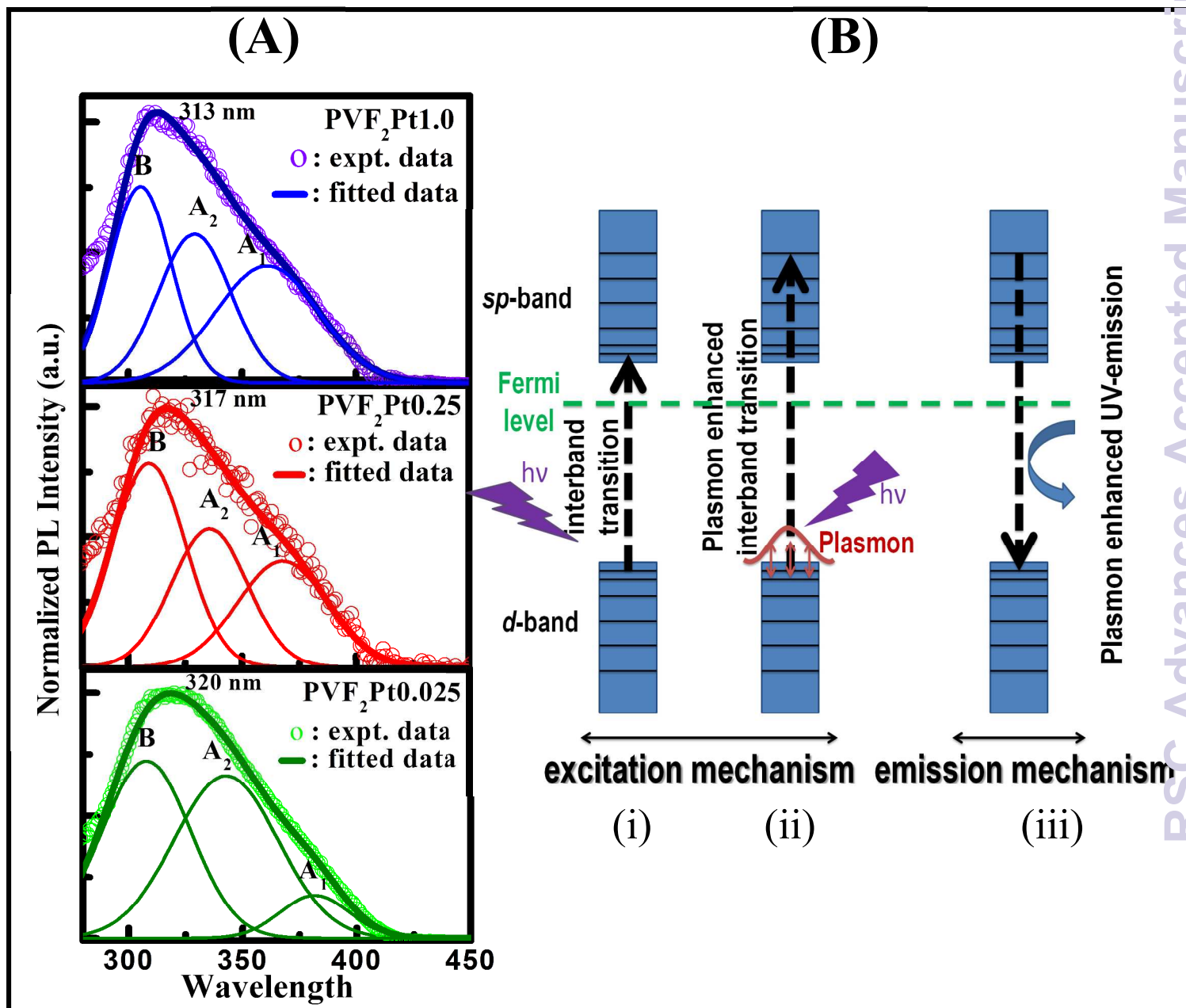


Fig. 9 (A) The room temperature normalized PL spectrum of Pt-NPs doped PVDF films. (B) A schematic diagram of excitation and emission mechanism [(i) excitation due to only interband transition and (ii) due to Plasmon enhanced interband transition, (iii) due to Plasmon enhanced UV-emission] to represent the UV- photoemission from Pt-NPs doped PVDF films.

This UV-emission is probably due to the coupling effect between LSPR and *d-sp* interband transition.³⁹ The enhancement of interband transition followed by the plasmons coupling (shown by the schematic diagram of Fig. 9B (ii) & (iii)) of electronic transitions responsible for intense UV-emission. It should also be noted that the frequency of the LSPR of platinum is located in the ultraviolet region⁴³⁻⁴⁴ and likewise we have also observed the strong *d-sp* interband transition of Pt-NPs as evident from UV-vis absorption spectra (shown in Fig. 2c). Thus, under the UV-light excitation (shown in Fig. 9B (ii)) both *d-sp* interband transition of single electron and surface Plasmon absorption also may occur, as a consequence, coupling between LSPR and interband transition gives rise Plasmon enhanced UV-emission (as shown in schematic of Fig. 9B (iii)). Thus Pt-NPs doped PVDF film promises a new type of photonic application apart from its electroactive activity, extends its importance as potential multifunction film for versatile sensor fabrication.

CONCLUSIONS

The multifunctional Pt-NPs doped PVDF films are prepared using a simple solvent casting technique. By simply controlling the platinum precursor amount, almost complete conversion (99 %) to electroactive phases is achieved as evident from spectroscopic and crystallographic information. In other words, we have proposed a simple method of *in-situ* Pt-NPs synthesis that might have enormous advantage over a typical catalysis. In contrast to a typical catalysis, a new

type of catalytic role in crystalline phase conversion in PVDF, *i.e.*, from non-polar α -phase to electroactive β and γ -phases is noticed. The overall crystallinity (χ_c) is reduced upon Pt-NPs doping and more importantly, piezoelectric β - crystallinity (χ_β) is considerably improved. This signifies high dielectric strength and can be used to build multilayer capacitors for energy storage. Furthermore, higher yield of β - crystallinity in Pt-NPs doped film promotes considerable higher (4 times) remnant polarization in comparison to the neat PVDF film, indicating an improved ferroelectric properties for non-volatile memory. In this work, we have also shown that tactile sensors made with un-poled Pt-NPs doped PVDF films exhibiting ultra-sensitive human finger touch response, possibly eliminating the traditional electrical poling steps. A considerable enhancement (~ 16 times) of rectified output voltage is realized upon Pt-NPs doping in PVDF. Potentially, these tactile sensors could be used to harvest energy and power small portable and wearable electronic devices. The PL-properties of Pt-NPs doped PVDF film aid an additional new avenue in photonic to be utilized as a flexible UV-emitter.

AUTHOR INFORMATION

Corresponding Author

*E-mail: dipankar@phys.jdvu.ac.in, Tel: +91-94333-73530. Fax: +91-33-2413-8917.

Notes. The authors declare no competing financial interest.

ACKNOWLEDGMENTS

Authors are grateful to DST, Govt. of India for developing instrumental facilities under FIST-II programme and providing the INSPIRE fellowship (IF130865) to Sujoy Kumar Ghosh. We are also thankful to Mr. Samiran Garain for his skillful FE-SEM operation and Mr. Biswajit Mahanty for demonstrating the way of optimized electrical signal recording.

REFERENCES

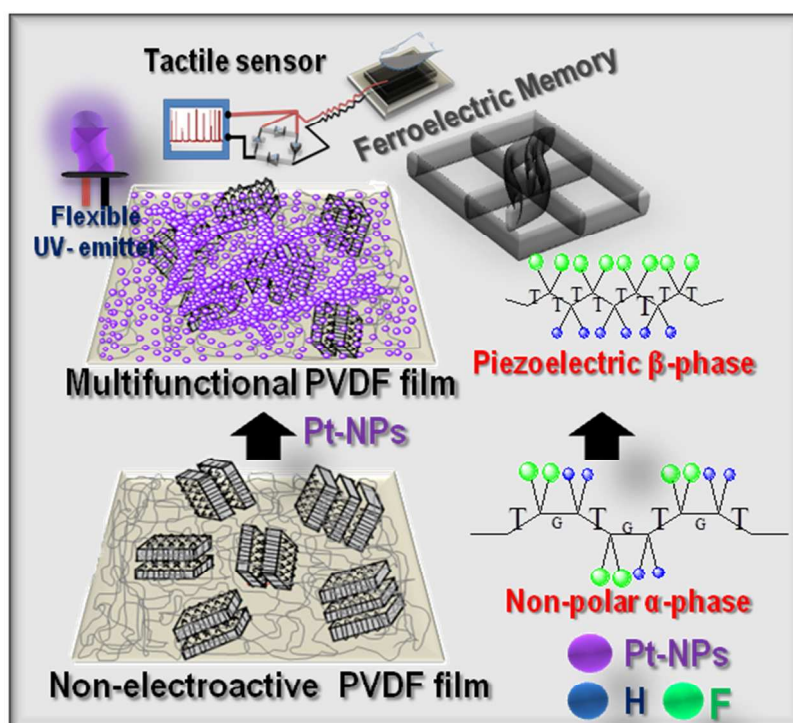
1. Z. L. Wang, *J. Phys. Chem. Lett.*, 2010, **1**, 1388-1393.
2. A. J. Lovinger, *Science*, 1983, **220**, 1115-1121.
3. K. Müller, D. Mandal, K. Henkel, I. Paloumpa, and D. Schmeisser, *Appl. Phys. Lett.*, 2008, **93**, 112901-1-3.
4. D. Mandal, K. J. Kim, and J. S. Lee, *Langmuir*, 2012, **28**, 10310-10317.
5. P. Martins, A. C. Lopes, S. Lanceros-Mendez, *Pro. Poly. Sci.*, 2014, **39**, 683-706.
6. W. Li, Q. Meng, Y. Zheng, Z. Zhang, W. Xia, and Z. Xu, *Appl. Phys. Lett.*, 2010, **96**, 192905-1-3.
7. M. Segev-Bar, and H. Haick, *ACS Nano*, 2013, **7**, 8366-8378.
8. S. Mourdikoudis, M. Chirea, T. Altantzis, I. Pastoriza-Santos, J. P'erez-Juste, F. Silva, S. Balsc, and L. M. Liz-Marz'an, *Nanoscale*, 2013, **5**, 4776-4784.
9. D. Mandal, K. Henkel, and D. Schmeißer, *Mater. Lett.*, 2012, **73**, 123-125.
10. C. Xu, K. J. Kim, Y. Wang, S. Yoon, G. Ren, D. Mandal, and B. Li, In Flexible Nanogenerator and Nano-Pressure Sensor Based on Nanofiber Web of PVDF and its Copolymers, in *Soft Fibrillar Materials: Fabrication and Applications* (Eds: Liu, X. Y., J.-L. Li, J. L.), Wiley-VCH, Weinheim, Germany, 2013, p233-264.
11. P. Zhang, X. Zhao, X. Zhang, Y. Lai, X. Wang, J. Li, G. Wei, Z. Su, *ACS Appl. Mater. Interfaces* 2014, **6**, 7563-7571.
12. M. Ahmad, and J. Zhu, *J. Mater. Chem.*, 2011, **21**, 599-614
13. O. D. Jayakumar, N. Manoj, V. Sudarsan, C. G. S. Pillai, and A. K. Tyagi, *Cryst Eng Comm*, 2011, **13**, 2187-2190.

14. W. Kaifeng, Z. Haiming, L. Zheng, R. William, and L. Tianquan, *J. Am. Chem. Soc.*, 2012, **134**, 10337-10340.
15. N. Mazumder, D. Sen, S. Saha, U. K. Ghorai, N. S. Das, and K. K. Chattopadhyay, *J. Phys. Chem. C*, 2013, **117**, 6454–6461.
16. J. B. You, X. W. Zhang, J. J. Dong, X. M. Song, Z. G. Yin, N. F. Chen, and H. Yan, *Nanoscale Res. Lett.*, 2009, **4**, 1121–1125.
17. C. Y. Kang, C. H. Chao, S. C. Shiu, L. J. Chou, M. T. Chang, G. R. Lin, and C. F. Lin, *J. Appl. Phys.*, 2007, **102**, 073508-073515.
18. V. Sencadas, P. Martins, A. Pitães, M. Benelmekki, J. Ribelles, and S. Lanceros-Mendez, *Langmuir*, 2011, **27**, 7241-7249
19. L. Li, M. Zhang, M. Rong, and W. Ruan, *RSC Adv.*, 2014, **4**, 3938–3943.
20. V. K. Tiwari, D. K. Avasthi, and P. Maiti, *ACS Appl. Mater. Interfaces*, 2011, **3**, 1398-1401.
21. H. J. Ye, L. Yang, W. Z. Shao, Y. Li, S. B. Sun, and L. Zhen, *RSC Adv.*, 2014, **4**, 13525–13532,
22. P. Zapata, D. Mountz, and J. C. Meredith, *Macromolecules* 2010, **43**, 7625–7636.
23. Z. Kónya, V. F. Puentes, I. Kiricsi, J. Zhu, P. Alivisatos, and G. A. Somorjai, *Catal. Lett.* 2002, **81**, 137-140.
24. N. Viet-Long, O. Michitaka, N. N. Van, C. Minh-Thi, and N. Masayuki, *Adv. Nat. Sci.: Nanosci. Nanotechnol.*, 2012, **3**, 025005-025008.
25. R. C. Johnson, J. Li, J. T. Hupp, and G. C. Schatz, *Chem. Phys. Lett.*, 2002, **356**, 534–540.
26. Jr. R. Gregorio, and C. Marcelo, *J. Poly. Sci.: Part B: Polymer Physics*, 1994, **32**, 859-870.
27. B. S. Ince-Gunduz, R. Alpern, D. Amare, J. Crawford, B. Dolan, S. Jones, R. Kobylarz, M. Reveley, and P. Cebe, *Polymer*, 2010, **51**, 1485-1493.

28. Y. Kang, M. Li, Y. Cai, M. Cargnello, R. E. Diaz, T. R. Gordon, N. L. Wieder, R. R. Adzic, R. J. Gorte, E. A. Stach, and C. B. Murray, *J. Am. Chem. Soc.* 2013, **135**, 2741–2747.
29. D. Mandal, K. Henkel, and D. Schmeisser, *J. Phys. Chem. B*, 2011, **115**, 10567-10569.
30. Jr. R. Gregorio, and D. S. Borges, *Polymer*, 2008, **49**, 4009-4016.
31. C. R. Bowen, H. A. Kim, P.M. Weaver, and S. Dunn, *Energy Environ. Sci.*, 2014, **7**, 25–44.
32. D. Lingam, A. R. Parikh, J. Huang, A. Jain, and M. M.-Jolandan, *Int. J. Smart Nano Mate.*, 2013, **4**, 229-245.
33. D. Mandal, K. Henkel, and D. Schmeißer, *Phys. Chem. Chem. Phys.*, 2014, **16**, 10403-10407.
34. M.Y.F. Elzayat, S. El-Sayed, H.M. Osman, and M. Amin, *Polym. Eng. Sci.*, 2012, **52**, 1945–1950.
35. F. Guan, J. Wang, J. Pan, Q. Wang, and L. Zhu, *Macromolecules*, 2010, **43**, 6739–6748.
36. W. Heywang, K. Lubitz, and W. Wersing, Piezoelectricity: Evolution and Future of a Technology, (*Editors: R. Hull, Jr. R.M. Osgood, J. Parisi, H. Warlimont*), Springer Series in Materials Science, 2008, p 157-176, ISBN 978-3-540-68680-4.
37. Z. Li, X. Zhang, and G. Li, *Phys. Chem. Chem. Phys.*, 2014, **16**, 5475—5479.
38. X. Xue, S. Wang, W. Guo, Y. Zhang, and Z. L. Wang, *Nano Lett.*, 2012, **12**, 5048–5054
39. J. Zheng, C. Zhou, M. Yu, and J. Liu, *Nanoscale*, 2012, **4**, 4073-4083.
40. H. Kawasaki, H. Yamamoto, H. Fujimori, R. Arakawa, M. Inada, and Y. Iwasaki, *Chem. Commun.*, 2010, **46**, 3759-3761.
41. S. Link, and M. A. El-Sayed, *Annu. Rev. Phys. Chem.*, 2003, **54**, 331-66.
42. A. Mooradian, *Phys. Rev. Lett*, 1969, **22**, 185-187.
43. H.-T. Sun, and Y. Sakka, *Sci. Technol. Adv. Mater.*, 2014, **15**, 014205-014218.
44. C. Langhammer, Z. Yuan, and I. Zoric', and B. Kasemo, *Nano Letters*, 2006, **6**, 833-838.

Table of Contents (TOC)

The *in-situ* formation of platinum nanoparticles and its catalytic role in electroactive phase formation in poly(vinylidene fluoride): A simple preparation of multifunctional poly(vinylidene fluoride) films doped with platinum nanoparticles



This work demonstrates multifunctional properties from PVDF films doped with Pt-NPs. A simple methodology of *in-situ* Pt-NPs is proposed and a new catalytic role of crystalline phase transformation from non-polar α -phase to electroactive β and γ -phase is observed. The ultra touch sensitivity from the human finger, high ferroelectric remnant polarization and UV-photoluminescence from PVDF film doped with Pt-NPs promises its versatile utility. Furthermore, high piezoelectric β -phase content also indicates to have applications as vibration and temperature based energy harvesters.